The El Niño Southern Oscillation in the Pliocene: Modelling water isotopes and implications for data interpretation.

Abstract

TO REWRITE Model simulations using the isotope enabled version of the Hadley Centre GCM (HadCM3) are used to evaluate where the El Niño Southern Oscillation (ENSO) could be detected in $\delta^{18}O$ from archives of Pliocene age. Results suggest that pristine Pliocene corals would usually have similar skill in the Pliocene and the Preindustrial, however regions with a strong El Niño precipitation signal would be better represented in Pliocene aged data. In general, ENSO can be better detected in individual Planktonic foraminifera data of Pliocene age than of pre-industrial age, since the signal to noise ratio is larger. However, spurious results can arise when a data site is close to a large spatial gradient in climate. One case study found that modelled foraminifera data from the Eastern Pacific could be used to accurately detect El Niño in the preindustrial, but not in the Pliocene, due to changes in the variability of $\delta^{18}O_{sw}$ and shifts in the upwelling zones between the two climates. This study shows that testing a method of proxy interpretation on modern data is not sufficient indication that the method is valid for the Pliocene. It also highlights that the location of data sites should be chosen with extreme care in order to avoid unreliable results.

1 Introduction

The El Niño Southern Oscillation (ENSO) is the strongest signal of interannual variability in the ocean-atmosphere system (*Wang et al.*, 1999). Greater predictability of ENSO leads to greater predictability of climate extremes such as floods and droughts (*Goddard and Dilley*, 2005) and potentially the associated socioeconomic impacts. However there has been some disagreement between models as to how ENSO will change in a warming climate (*Latif and Keenlyside*, 2009, *Collins et al.*, 2010), and the future behaviour of ENSO is still uncertain.

One way to examine ENSO in a warmer than modern climate, is to look to warmer climates of the past. A period which has received much attention is the mid-Pliocene Warm Period (mPWP). This occurred 3.264-3.025Ma and represents a relatively familiar world with continental configuration similar to modern and CO_2 levels close to the current value of 400ppmv (*Stap et al.*, 2016, *Seki et al.*, 2010). However unlike the constantly warming climate that exists today, the mPWP was warm and stable. It had global annual mean sea surface temperatures 2-3°C higher than pre-industrial (*Dowsett et al.*, 2010, *Haywood et al.*, 2000) and polar ice reduced by up to 1/3 (*Dolan et al.*, 2011).

The behaviour of ENSO in the mPWP is subject to a great deal of debate and uncertainty. However, unlike future ENSO uncertainties, there are datasets from the mPWP on which this debate can be based. Many studies have argued for protracted Pliocene El Niño conditions (referred to as a 'permanent El Niño) (e.g. *Molnar and Cane*, 2002, *Philander and Fedorov*, 2003, *Fedorov et al.*, 2006). This has been based on a reduced east-west temperature gradient across the Pacific (e.g. *Wara et al.*, 2005), lower productivity/reduced upwelling in the eastern equatorial Pacific (*Seki et al.*, 2012), or climate patterns consistent with modern El Niño teleconnections (*Winnick et al.*, 2013).

The reduced east-west temperature gradient across the Pacific (*Wara et al.*, 2005), relies on proxy data which suggests that the eastern equatorial Pacific (EEP) was warmer than today while the western equatorial Pacific (WEP) was not. However, *Zhang et al.* (2014a) used different proxies from the same WEP site which suggested that the WEP was also warmer than today and a similar E-W temperature gradient existed. Whether or not an E-W temperature gradient existed in the Pliocene is still not resolved (*Ravelo et al.*, 2014, *Zhang et al.*, 2014b).

Studies which support suggestions of a permanent El Niño are not consistent in the dataing. *Steph et al.* (2010) suggested that the shallow thermocline (which has been associated with protracted El Niño) occurred earlier than previously suggested. It is likely that at least some of the Pliocene experienced ENSO variability similar to today, as *Watanabe et al.* (2011) found clear ENSO variability in two fossil corals form the Western Pacific, which were dated to approximately 3.5-3.8Ma. The fossil corals were analysed based on 12 samples per year for 35 years and so variability can be clearly measured. In addition *Scroxton et al.* (2011) found ENSO variability when considering measurements on individual planktonic foraminifera.

Modelling studies generally agree that there was ENSO related variability in the Pliocene (*Haywood et al.*, 2007, *Bonham et al.*, 2009, *von der Heydt et al.*, 2011, *Zhang et al.*, 2012, *Brierley*, 2015). However simulations from complex atmosphere-ocean general circulation models (AOGCM's) cannot apply to the whole Pliocene, and can only suggest ENSO variability for a shorter time period within the Pliocene. The time period used has generally been representive of the mPWP (3.264-3.025Ma), however *Haywood et al.* (2013) has argued that this is too broad for climate modelling purposes and a focus on an even shorter timeslice would be more appropriate.

In the same way that models do not agree on how ENSO behaviour will change in the future, neither do they fully agree on how ENSO was different in the Pliocene. However, models do appear to share some common features in their retrodiction of ENSO behaviour. *Brierley* (2015) considered 9 models used in the Pliocene Intermodel Comparison Project (PlioMIP), none of the models showed a 'permanent' El Niño, and there was a general conensus that there was less ENSO related variability with a shift to lower frequencies and reduced amplitude in the Pliocene. However *Tindall et al.* (2016) found that intra-model variability could exist within a single simulation, and suggested that there was likely to be centennial scale variability in ENSO strength for the Pliocene in the same way that there is for the modern (*Wittenberg*, 2009, *Li et al.*, 2011). Following a 2500 year spinup *Tindall et al.* (2016) found an increased amplitude of El Niño, even though there were shorter subsects of the simulation (200 years) in which the amplitude appeared to be reduced. It was however found that the intramodel variability was particularly limited to temperature in the Eastern Pacific, and that the centennial scale variability was less important for precipitation or temperature in the central or western Pacific.

Overall there are still substantial uncertainties in the behaviour of Pliocene ENSO, and reducing these uncertainties could lead to a better understanding of ENSO in a warm climate. The uncertainties exist in both model and data, and it is difficult to compare the two due to the very different nature of what each can derive. GCM's provide climate indicators at a global scale for a relatively short timescale (e.g 3.205Ma, *Haywood et al.*, 2013), while data is gathered from a very limited number of locations over a very long timescale (e.g. 'A 12 million-year temperature history...' *Zhang et al.*, 2012). In addition the derived quantities are not always directly comparable. For example the temperature and precipitation that is output from climate models is not directly measured in paleoarchives and is instead inferred from other quantities (e.g. magnesium calcium ratios, the alkenone unsaturation index, TEX_{86} or the ratio of water isotopes). To better compare model and data it is necessary to either convert data measurements into quantities measured by the model using a transfer function (e.g *Erez and Luz*, 1983, *Dekens et al.*, 2002), or alternatively for the model to directly simulate the quantity measured in the archive. Recent years have seen a large increase in the number of models able to simulate one such measured quantity, namely stable water isotope tracers (e.g. *Lee et al.*, 2007, *Roche*, 2013, *Haese et al.*, 2013, *Dee et al.*, 2015). This can be used to better compare model and δ^{18}O measured in paleoarchives (e.g *Tindall et al.*, 2010, *Roberts et al.*, 2011, *Holmes et al.*, 2016). For the mPWP, the Hadley Centre GCM, HadCM3, has been run with water isotope tracers included, to increase synergy between model and data (*Tindall and Haywood*, 2015), however so far only the global large scale features have been discussed.

Here we will use the water isotope enabled version of HadCM3 to investigate ENSO based on observed and simulated δ^{18}O in the Pacific ocean. The aims are: 1. to compare model results with existing proxy data to investigate the accuracy of ENSO signals in the data, and 2. to directly simulate proxy measurements throughout the Pacific and highlight regions where proxy data of Pliocene age could provide a good representation of ENSO. For necessity we will limit model-data comparison to archives which contain δ^{18}O measurements and will also concentrate mainly on data with high temporal resolution, such as the coral data of *Watanabe et al.* (2011) and the individual planktonic foraminifera analysis of *Scroxton et al.* (2011). This is because GCM's are run at very high temporal resolution and such a comparison allows a more comprehensive data-model comparison which is not just based on one single datapoint in time.

In Section 2 we will describe the model and simulations used to simulate δ^{18}O for the Pliocene climate. Section 3 will discuss El Niño Southern Oscillation (ENSO) climate modes and show how these could appear in Pliocene climate, δ^{18}O fields. Sections 4 and 5 will use the model results to reinterpret proxy data from corals and planktonic foraminifera respectively. In particular we will be assessing what information about ENSO can be derived from these archives, and locations where these archives would give the most reliable indication of El Niño behaviour. A discussion of the results and the conclusions are presented in section 6.

2 Methods

2.1 Model description

The model used in this study is the Hadley Centre General Circulation Model (HadCM3; *Gordon et al.*, 2000, *Pope et al.*, 2000) with water isotope tracers included throughout the hydrological cycle (*Tindall et al.*, 2009). HadCM3 has resolution of 3.75°× 2.5° with 19 vertical levels in the atmosphere, and 1.25°× 1.25° with 20 vertical levels in the ocean. HadCM3 uses the *Gregory and Rowntree* (1990) convection scheme, a large scale cloud scheme based on *Smith* (1990) with modifications described by *Gregory and Morris* (1996), and the *Edwards and*

Slingo (1996) radiation scheme. In the ocean HadCM3 comprises a simple sea ice model, which is based on the zero-layer model of *Semtner* (1976) (and includes ice drifts, leads and snow cover). The version of the HadCM3 used here comprises the MOSES2 land surface exchange scheme which includes the TRIFFID dynamic vegetation model (*Cox et al.*, 1999) such that the vegetation is predicted by the model rather than prescribed.

HadCM3 has been used in a number of studies of the mPWP (e.g. *Hill*, 2015, *Pound et al.*, 2014, *Dolan et al.*, 2011) and in particular has been run as part of the Pliocene Model Intercomparison Project (PlioMIP; *Bragg et al.*, 2012, *Haywood et al.*, 2013). HadCM3 is generally in good agreement with reconstructions although it underpredicts the Pliocene warming over the North Atlantic region (*Prescott et al.*, 2014) and the northern hemisphere high latitude terrestrial warming (*Salzmann et al.*, 2013).

The water isotope component of HadCM3 has been shown to provide a good representation of the δ^{18}O of seawater ($\delta^{18}O_{sw}$) and the δ^{18}O of precipitation ($\delta^{18}O_p$) for the pre-industrial climate (*Tindall et al.*, 2009), and has recently been used to investigate the large scale features of $\delta^{18}O_{sw}$ and $\delta^{18}O_p$ for the mPWP (*Tindall and Haywood*, 2015). HadCM3 suggests that over many regions,the long term average, mPWP $\delta^{18}O_{sw}$ was similar to that predicted by correcting preindustrial $\delta^{18}O_{sw}$ values by Pliocene ice volume. The more intensive hydrological cycle led to regional $\delta^{18}O_{sw}$ anomalies from an ice volume correction over coastal regions, the south Atlantic and the Arctic, however throughout the equatorial Pacific an ice volume correction was mainly sufficient for estimating Pliocene $\delta^{18}O_{sw}$.

HadCM3 simulates a present day ENSO with amplitude and frequency broadly in agreement with observations, and its skill compares well with other CMIP3 and CMIP5 models (*Bellenger et al.*, 2014). *Tindall et al.* (2009) considered the pre-industrial El Niño signature in HadCM3 for precipitation amount, $\delta^{18}O_p$ and $\delta^{18}O_{sw}$. Although over much of the tropics precipitation anomalies compare well with observations (*Dai and Wigley*, 2000, *AchutaRao and Sperber*, 2002) the model fails to simulate the full extent of the dry conditions of El Niño that occur in the western Pacific warm pool, which leads to errors in the extent of $\delta^{18}O_p$ and $\delta^{18}O_{sw}$ in this region. In the location of the western Pacific warm pool, in particular, extreme care must be taken when using HadCM3 results to interpret paleodata from a fixed location (or paleoproxy site), and while the model is indicative of what an El Niño $\delta^{18}O_{sw}$ signal would look like in a dry or wet region, spatial results will only apply in a broad sense.

2.2 Experimental Design

The HadCM3 experiments with δ^{18}O tracers analysed here were previously used by *Tindall and Haywood* (2015), and include a mPWP experiment and a pre-industrial control. Both simulations were run for 2500 years and were initialised from a preindustrial experiment that had been run for several millenia with δ^{18}O tracers. The boundary conditions for the mPWP experiment are from the Pliocene research, Interpretation and Synoptic Mapping project (PRISM *Dowsett et al.*, 1994), with ice sheets, orography and initial vegetation parameters from the PRISM3D version (*Dowsett et al.*, 2010) which was used for PlioMIP. Orbital parameters are set to 3.205Ma (as suggested by *Haywood et al.*, 2013) and CO_2 levels are set to 405ppmv. Since mPWP $\delta^{18}O_{sw}$ was intialised, unchanged, from the end of a long pre-industrial simulation it is necessary to reduce this value at a postprocessing stage to account for the reduced Pliocene ice sheets. Following *Tindall and Haywood* (2015) $\delta^{18}O_{sw}$ is reduced by 0.3‰ corresponding to the ice sheet reduction of 1/3 that was included in the simulation.

El Niño and La Niña months were detected in these simulations based on the Oceanic Nino Index (ONI), which is used by NOAA's Climate Prediction Center. The ONI is the three month running mean SST anomaly in the NINO3.4 region; when the ONI exceeds a threshold of +0.5°C for at least 5 consecutive months it is categorised as El Niño, when the ONI is below -0.5°C for at least 5 consecutive months it is categorised as La Niña. Months that are neither El Niño or La Niña are categorised as 'neutral'. All El Niño/La Niña/neutral months are then combined into El Niño/La Niña/neutral composites, after weighting each month's contribution such that each composite included the same amount of information from each calendar month. This paper will mainly consider El Niño and La Niña in the final 300 years (years 2200-2500) of the simulations. This is where the simulations are closest to a fully spun-up state and these years are representative of the majority of the simulations.

3 The El Niño Southern Oscillation in the Pliocene

Using the definition based on the ONI (see methods), the temperature, precipitation $\delta^{18}O_p$ and $\delta^{18}O_{sw}$ anomalies for El Niño minus neutral conditions were produced. These are shown in figure 1 for the preindustrial (left), the Pliocene (centre) and the difference between them (right). It is seen that for all fields considered the HadCM3 El Niño anomaly is stronger in the Pliocene than in the pre-industrial. Relative to the pre-industrial the magnitude of the Pliocene El Niño anomaly is approximately 28% larger for temperature, 32% larger for precipitation, 29% larger for $\delta^{18}O_p$ and 37% larger for $\delta^{18}O_{sw}$, although there is spatial variability in these numbers (particularly for temperature). This suggests that, unless the amplitude of non-ENSO climate signals has similarly increased, the signal to noise ratio of ENSO events in the Pliocene was larger than preindustrial and may be more easily detectable in Pliocene aged proxy data. However *Tindall et al.* (2016) showed that there is centennial scale variability in the strength of ENSO, both in the preindustrial and the Pliocene, such that the generally increased ENSO strength in the Pliocene is not ubiqutous. In particular intra-model variability means that ENSO was not consistently stronger in the Pliocene in the NINO3.4 region or the Eastern part of the Pacific. However temperature signals in the western half of the Pacific and precipitation signals (following through to $\delta^{18}O_p$ and $\delta^{18}O_{sw}$) signals were consistently stronger in the Pliocene simulation.

In the next sections we will discuss how the El Niño temperature and $\delta^{18}O_{sw}$ signals, seen in HadCM3 would combine within a proxy archive and what information about ENSO we would be able to gather from that archive. In particular we discuss whether the ability to detect ENSO in $\delta^{18}O$ measured in a Pliocene aged archive is likely to be different from the Preindustrial.

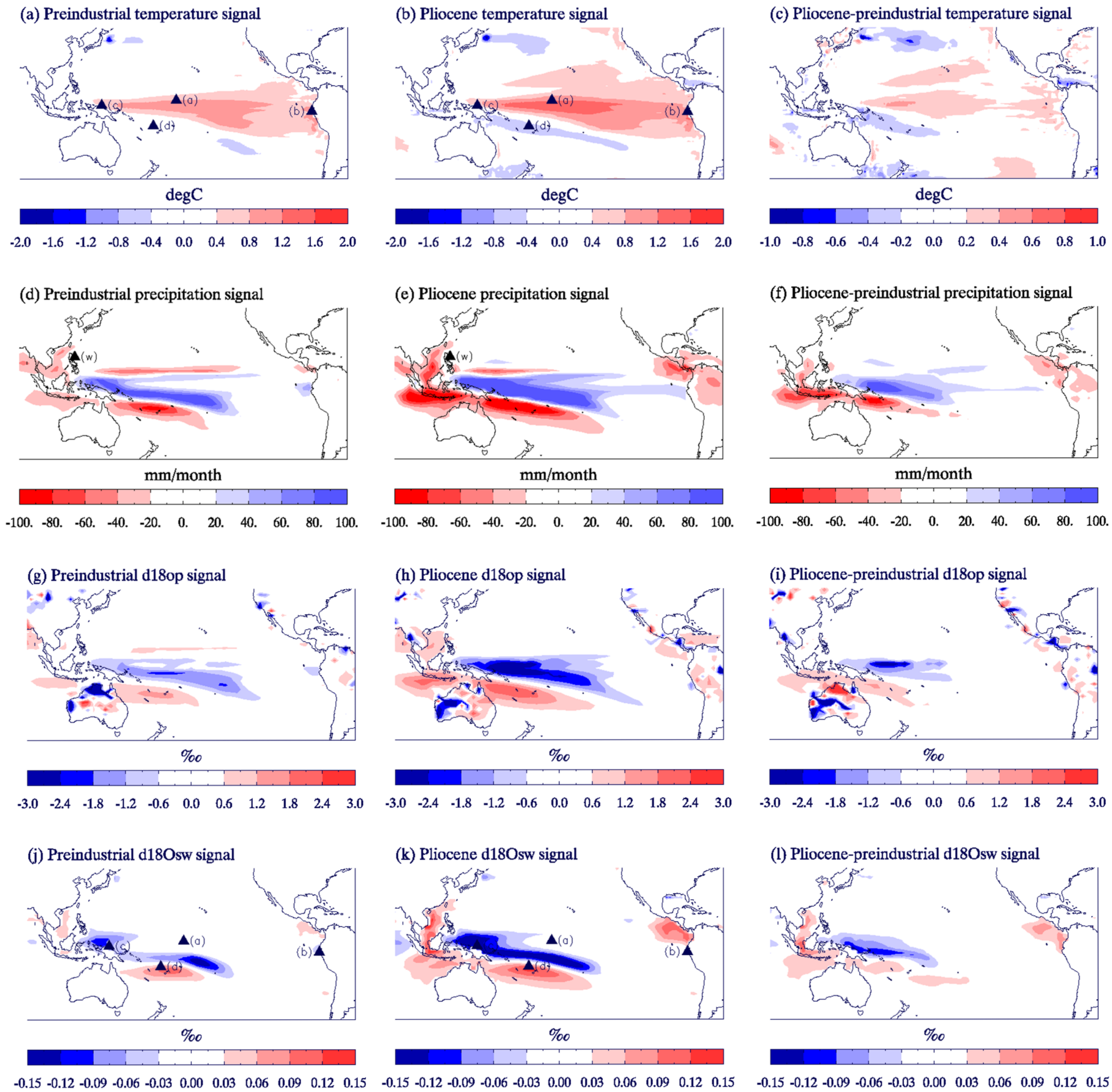

Figure 1: pre-industrial (left) and Pliocene (centre) anomalies between El Niño and neutral climate states. The difference between the Pliocene El Niño anomalies and the Preindustrial anomalies (centre figures minus left figures) are also shown (right).

4 Comparison to coral data

To assess El Niño, it is beneficial to have climate proxy data of high temporal resolution. The coral data of *Watanabe et al.* (2011) (extracted from two 35 year corals in the Philippines) has monthly resolution - which is the highest available for the Pliocene. A spectral analysis of the δ^{18}O of these corals showed spectral peaks that correspond to present day ENSO variability. In addition δ^{18}O from a nearby, live, coral correlated well with modern records of ENSO and negative δ^{18}O events in the fossil coral resemble negative δ^{18}O events in the live coral. The evidence from these corals suggest Pliocene ENSO variability similar to modern.

In theory, this coral data is ideal for validating the HadCM3 Pliocene isotope simulations and also for combining model and data to better understand Pliocene El Niño. However these corals are from a region of the Western Pacific where HadCM3 fails to reproduce the dry conditions associated with El Niño, either for the Pliocene or the pre-industrial (see (w) on figure 1d and e). This means that a site to model gridbox data-model comparison of these corals would be unable to provide information about the modelled ENSO, nor could it help the model to interpret ENSO signatures in the data. However the coral data can still be used to validate the annual average and non-ENSO (e.g. seasonal) related variability of $\delta^{18}O_C$ simulated by the model. To understand what information about ENSO could be determined from coral in a region with a 'dry' El Niño signal an alternative region of the Pacific where El Niño precipitation patterns are better represented by the model will later be discussed.

Figure 2 compares the coral data of *Watanabe et al.* (2011), to HadCM3 pseudocoral $\delta^{18}O_c$ produced from the nearest gridbox (14.375°N, 124°E). The pseudocoral $\delta^{18}O_c$ is produced by combining modelled temperature with modelled $\delta^{18}O_{sw}$ according to the equation of *Juillet-Leclerc and Schmidt* (2001) which is:

$$T = 2.25 - 5(\delta^{18}O_c - \delta^{18}O_{sw}) \quad (1)$$

Even though the spectral peak at ENSO frequencies that occurs in the coral data is absent from our pseudocoral $\delta^{18}O_c$ (not shown), there appears to be excellent model-data agreement on other timescales at this location. Both the mean and annual variability in δ^{18}O agree well between the modelled coral and the observed coral, and the magnitude of the interannual variability (obtained after removing the annual cycle) is reproduced by the pseudo coral. The general agreement between the *Watanabe et al.* (2011) coral and HadCM3 (figure 2) suggests that the model is able to provide a good representation of coral data of Pliocene age.

In order to use HadCM3 for interpreting coral ENSO signals we now derive HadCM3 pseudocorals from other locations, where the model better represents El Niño. These locations are shown on figure 1 (a, b, j and k) and are: two locations where there is a large temperature signal associated with ENSO (a) in the central Pacific (0°N, 190°E) and b) in the Eastern Pacific (7°S, 81°W); c) a gridbox in the Western Pacific (3°S, 141°E) which has increased precipitation (and hence a negative $\delta^{18}O_{sw}$ excursion) in El Niño years and d) a gridbox (16S°N, 175°E)

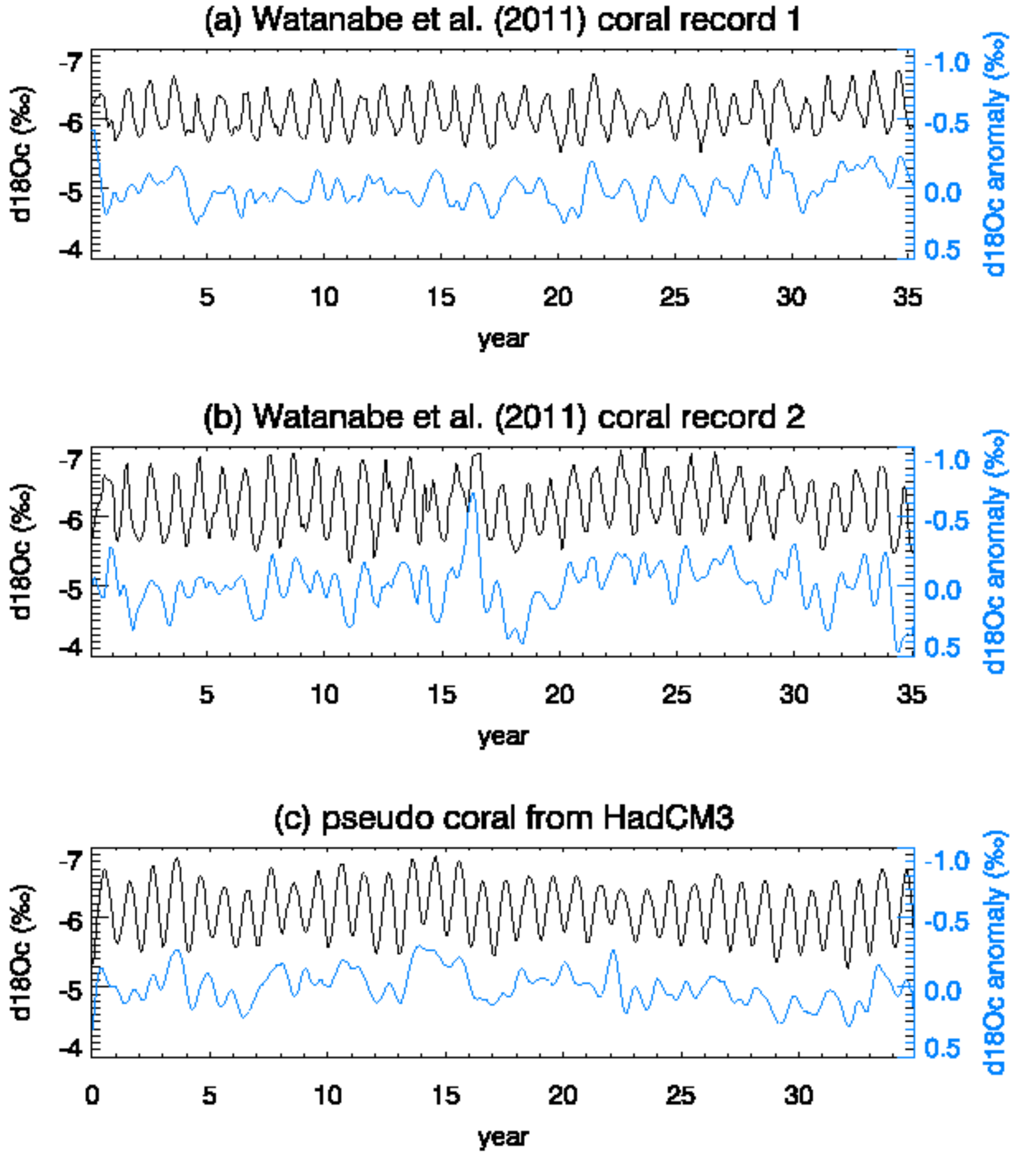

Figure 2: Coral data from *Watanabe et al.* (2011) and pseudo coral $\delta^{18}O_c$ obtained from HadCM3. Black line show absolute values and blue line show the anomaly obtained after removing the annual cycle and taking a 5 month running mean.

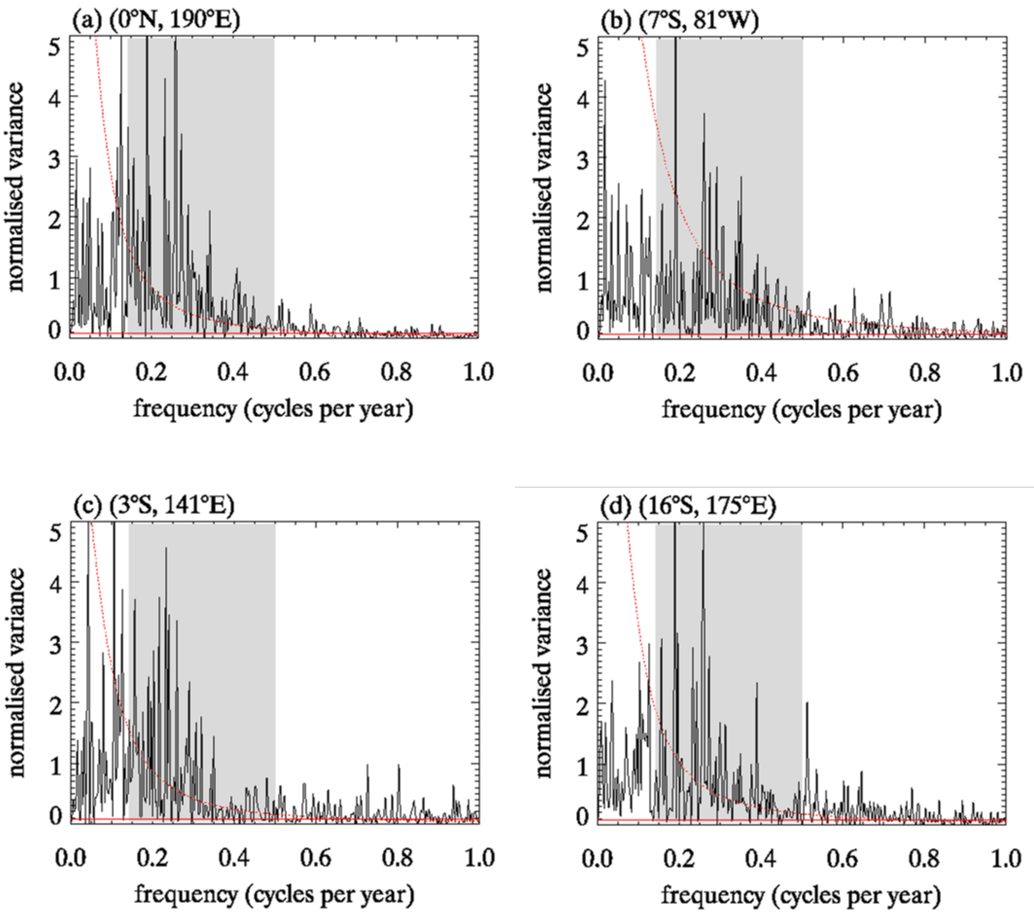

Figure 3: Power spectral analysis of a modelled coral from 4 sites, marked on figure 1. The shaded band highlights frequencies corresponding to the expected 2-7year period of ENSO. The red lines show the variance that could be attributed to red and white noise.

which has reduced precipitation in El Niño years. At each of these locations pseudocoral $\delta^{18}O_c$ is produced using equation 1.

Figure 3 shows the power spectrum of $\delta^{18}O_c$ from a 300 year pseudocoral $\delta^{18}O_c$ at these locations. The shaded bars show frequencies representing the 2-7 year period of expected ENSO variability, and the red lines show red and white noise with the same variance as the pseudocoral data. Since the pseudo-corals lie in ENSO regions they all exhibit spectral peaks at ENSO frequencies. However, the spectral peaks are not the same in every pseudo-coral, which implies that the skill of each pseudocoral in detecting ENSO signals will be different. Of these pseudocorals the strongest spectral peaks in $\delta^{18}O_c$ relative to the background lie in the central pacific (figure 3a), while the weakest spectral peaks are in the Eastern Pacific, due to more variability at non-ENSO frequencies. Spectral peaks in the precipitation regions (c and d) are of a similar magnitude).

We now consider whether true El Niño and La Niña events can be detected from any of these pseudo corals, and the likely accuracy in detection. For each of the four sites we show the pseudocoral $\delta^{18}O_c$ after removal of the average annual cycle (black line figure 4). Pseudocoral $\delta^{18}O_c$ was then used to infer El Niño and La Niña events based on the definition of *Leloup et al.* (2008) as follows. Firstly a thrshold t_{ENSO} is determined which corresponds to half of the standard deviation of the pseudocoral $\delta^{18}O_c$. El Niño and La Niña are inferred if pseudocoral $\delta^{18}O_c$ is more extreme than that threshold for at least 6 consecutive months. Times of the simulation when the pseudo-coral infers El Niño and La Niña are shown as red bars (El Niño) and blue bars (La Niña) that are plotted below the x-axis in figure 4. It can be seen that El Niño and La Niña are more often suggested by the simulation at location d) than elsewhere, while the pseudocoral at the central Pacific location (a) suggests less and generally shorter duration El Niño. Despite a notable overlap the same ENSO state is not inferred from the different pseudocorals.

A main advantage of using a climate model to simulate paleodata is that the model can simulate other climate features that occur simultaneously with the modelled paleodata. In this case 'true' El Niño and La Niña determined from the ONI can be obtained. Times when the model was in a 'true' state of El Niño and La Niña, are shown by the red and blue bars above the x-axis on figure 4. This means that bands which occur above and below the x-axis represent times when El Niño or La Niña has been correctly detected from the pseudocoral $\delta^{18}O_c$, bands that occur only above the axis represent times that El Niño or La Niña occurred in the model that could not be detected in the pseudocoral and bands that occur only below the x-axis represent times that the pseudo coral falsely suggests an El Niño or La Niña event. It can be seen that figure 4(a) which represents the central Pacific location is the point where El Niño can be best detected, here all events within the 50 years shown are correctly detected and few false events are inferred. At the other locations most of the El Niño/La Niña events are also correctly detected within the pseudocoral data, however there are a large number of events predicted that did not occur, particularly for the dry El Niño location (d).

The large number of false events seen on figure 4 questions whether the threshold chosen to infer ENSO was too low. It is noted that the exact threshold is unknown, and will likely change depending on the location of the pseudo-coral and the time period. While an alternative threshold may have been more appropriate for some locations, we have chosen not to tune the threshold value as such tuning would not be possible when interpreting paleodata. Also, the condition that the extreme values must persist for 6 consecutive months reduces the importance of the exact threshold chosen.

To extend the results from figure 4 we consider the number of El Niño and La Niña events that can be detected in the final 300 years of the Pliocene simulation. This is shown in Table 1, and supports the results in figure 4. Most of the El Niño and La Niña events within the 300 years can be detected using this method (albeit with a number of false positives).

For comparison table 1 also shows the number of ENSO events that could be detected in the corresponding pre-industrial simulation. It can be seen that overall a greater proportaion of El Niño and La Niña can be detected in the Pliocene pseudocorals than in corresponding pre-industrial pseudocorals and the proportion of falsely predicted events is smaller in the Pliocene than in the pre-industrial. The reason that El Niño events are easier to detect, from a single

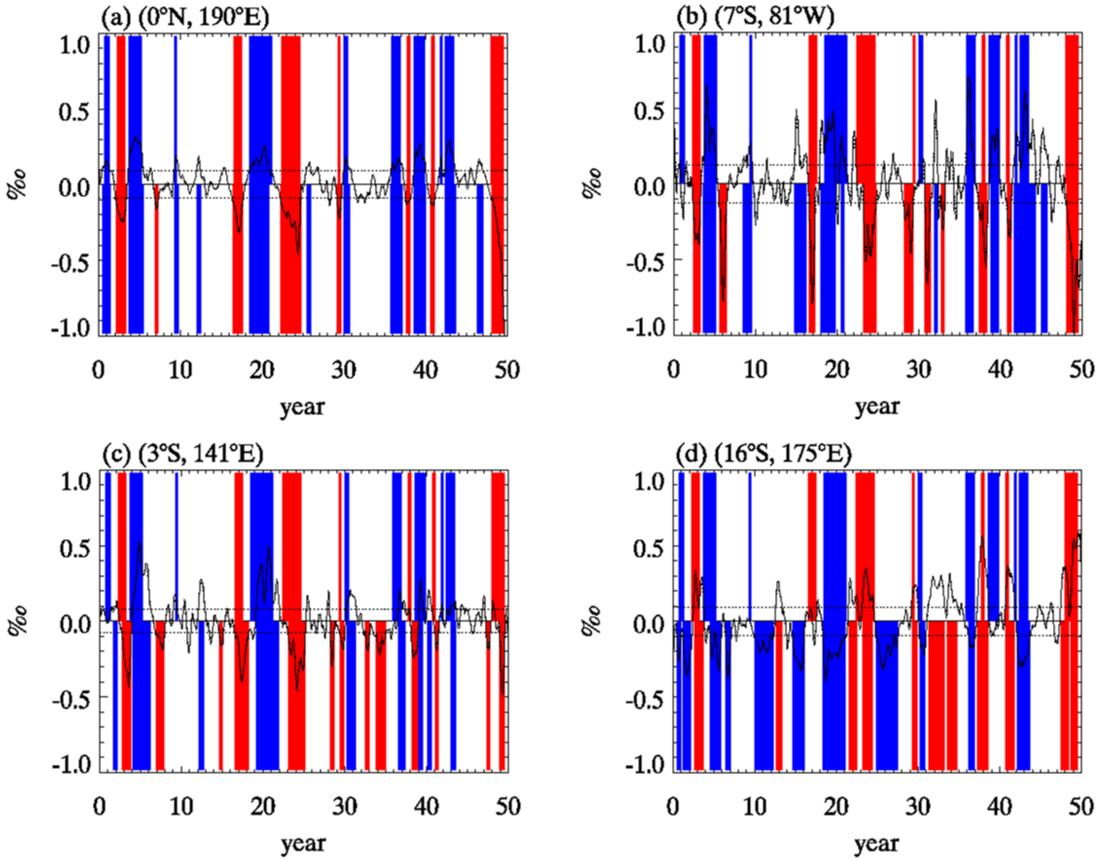

Figure 4: Modelled coral at 4 locations. Bands above the x-axis show times where El Niño (red) and La Niña (blue) were present in the simulation. Bands below the axis show times when El Niño (red) and La Niña (blue) were inferred from the pseudo coral at the location.

Pliocene				
location	phase	detected (as percentage of modelled events)	not detected	false positive (as percentage of predicted events)
0N, 190E	El Niño	41 (95%)	2	6 (13 %)
Central Pacific	La Niña	53 (98%)	1	18 (25%)
6.875S, 278.75E	El Niño	41 (95%)	2	19 (32 %)
Eastern Pacific	La Niña	48 (89%)	6	24 (33%)
3.125S, 141.25E	El Niño	37 (86%)	6	22 (37%)
-ve $\delta^{18}O_{sw}$ signal	La Niña	39 (72%)	15	21 (35 %)
15S, 175E	El Niño	38 (88 %)	5	23 (38 %)
+ve $\delta^{18}O_{sw}$ signal	La Niña	45 (83 %)	9	31 (41 %)
total across all phases and locations		342 (88 %)	46	164 (32%)

Pre-Industrial				
location	phase	detected	not detected	false positive
0N, 190E	El Niño	51 (100 %)	0	18 (26 %)
Central Pacific	La Niña	49 (98 %)	1	19 (27 %)
6.875S, 278.75E	El Niño	44 (86 %)	7	25 (36%)
Eastern Pacific	La Niña	36 (72 %)	14	35 (49%)
3.125S, 141.25E	El Niño	38 (74%)	13	35 (48%)
-ve $\delta^{18}O_{sw}$ signal	La Niña	34 (68%)	16	45 (57%)
15S, 175E	El Niño	40 (78 %)	11	24 (37 %)
+ve $\delta^{18}O_{sw}$ signal	La Niña	37 (74 %)	13	47 (56%)
total across all phases and locations		329 (81%)	75	248 (42 %)

Table 1: Ability to detect El Niño and La Niña in the model produced pseudo-coral $\delta^{18}O_c$ at a single location. Results are from the final 300 years of the Pliocene and the Preindustrial simulations.

site, in the Pliocene than in the pre-industrial is due to the fact that El Niño events are stronger, relative to the background variability in the Pliocene. There is also notable coherence between the Pliocene and the preindustrial results: those sites which have good skill for the preindustrial also have good skill for the Pliocene. If the results of this modelling study accurately represent ENSO behaviour, they suggest that ENSO can usually be detected from a single site in the Pliocene provided the site is suitable for detecting modern ENSO.

Table 1 and figure 4 both show the skill to be best at the central Pacific site (a), followed by the Eastern Pacific site (b). The sites with an ENSO precipitation signal (c and d) appear to show similar skill in table 1, which just compares the number of events. However from figure 4 the skill appears better at site c (which has increased precipitation in El Niño years) because the false positives at this location are of shorter duration. Considering these four sites only, the skill of ENSO detection appears only loosely related to the strength of the spectral peaks seen in figure 3. Although the spectral peaks were strongest in the central Pacific site (which had best skill) the spectral peaks were weakest in the Eastern Pacific site where the skill was also relatively good.

4.1 Application across the Tropical Pacific

The ability to detect ENSO in pseudocorals has so far been discussed in relation to four locations where there is a strong ENSO signal and good skill is expected. However the model is not limited to four locations. We are able to calculate δ^{18}O from many pseudo-coral to fully investigate where the model suggests there should be a strong and accurate ENSO signature in timeseries data of Pliocene age. We therefore produce a 300 year pseudo-coral using equation 1 for each gridbox across the Pacific. To compare locations each pseudocoral will be allocated a skill score based on its ability to detect ENSO. The skill score for each pseudocoral is calculated as follows:

$$skill = \left(\frac{1}{3}\left[\frac{EN_c}{EN_t} + \frac{LN_c}{LN_t} + \frac{NT_c}{NT_t}\right] - \frac{1}{3}\right) \times \frac{2}{3} \qquad (2)$$

where EN, LN and NT denote the number of El Niño, La Niña and neutral months repectively. Subscript c denotes the number of months of each type that were correctly attributed and subscript t denotes the total months of that type. Note that the skill score has been normalised by subtracting 1/3 from the average of correctly detected events and multiplying by 2/3. Normalising means that if the model performs no better than random chance, there is an expected skill of 0 and perfect predictability will have a skill of 1. Also note that when determining whether a month was correctly attributed a two month margin of error was allowed, such that a month would be classed as correctly attributed if it was within 2 months of the predicted state.

The skill of the pseudo corals across the Pacific is shown in figure 5 for the Preindustrial and the Pliocene. As expected from our four test pseudocorals, regions of high skill in the Preindustrial generally correspond to regions of high skill in the Pliocene, and the difference in skill between regions is much larger than the difference in skill between the two time periods.

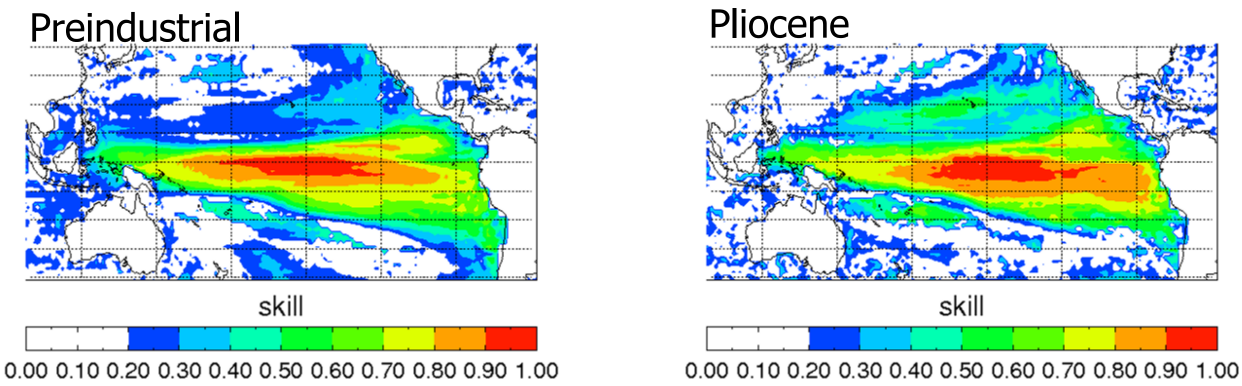

Figure 5: Skill of modelled 'pseudocorals' across the Pacific in their ability to detect ENSO. See text for a discussion of how the skill was calculated.

5 Comparison to planktonic foraminifera data

5.1 Bulk Foraminifera measurements

Although not able to provide a timeseries in the same way as coral data, previous work has used planktonic foraminifera data to assess El Niño changes between the Pliocene and the modern. Planktonic foraminifera data has been used in two main ways: 1.) a Bulk Foraminifera analysis where a number of foraminifera are crushed and mixed before analysis to find typical climate conditions. Data from bulk foraminifera analysis will be discussed in this section. 2.) The Individual foraminifer analysis, where a number of single formainifera are used to find the variability in climate. This will be discussed in section 5.2.

Wara et al. (2005) considered bulk foraminifera data from two sites, one from the Eastern Pacific and one from the Western Pacific. These suggested that the average temperature gradient across the Pacific was smaller in the Pliocene than the modern (2°C in the Pliocene, 6°C modern). They noted that the Pliocene average gradient was similar to modern "El Niño" conditions, and hypothesised that the Pliocene was in a permanent El Niño state. However their study also suggested that the thermocline depth in the Eastern Pacific from 4Ma-0Ma was similar to today, and not indicative of a permanent El Niño over this period. A permanent El Niño in the mid-Pliocene Warm Period does not agree with modelling studies (*Bonham et al.*, 2009, *Brierley*, 2015) or some other analyses (*Zhang et al.*, 2014a). Since this paper includes modelling of $\delta^{18}O_c$ in planktonic foraminifera, we revisit the comparison between the HadCM3 model and the *Wara et al.* (2005) study, in order to see if the two can be better reconciled.

The sites used in the *Wara et al.* (2005) study were ODP 806 (0°N,159°E) in the Western Pacific and ODP 847 (0°N,95°W) in the Eastern Pacific. Site ODP806 is the only published data of Pliocene age from the WEP warm pool (*Ravelo et al.*, 2014) and there is a great deal of controversy as to whether this site was warmer or not (*Ravelo et al.*, 2014, *Zhang et al.*, 2014b). Although most of this debate has been focussed on the early Pliocene (3.5-5Ma ago), the reasoning extends to the mPWP timeslice considered here. There is less controversy in the EEP. Studies generally agree that in the Pliocene this region was warmer than today. Due to a lack of data of Pliocene age, the sites used in the *Wara et al.* (2005) study are important locations for considering discrepencies in 'permanant El Niño' indicators.

Preindustrial HadCM3 does not reproduce the modern 6°C temperature difference calculated by *Wara et al.* (2005) between ODP806 and ODP847. Instead HadCM3 shows a temperature difference of 0.5°C at the surface and 4°C at 20m (20m being the depth represented by the data). The discrepency is partly due to the location of the sites. The Eastern Pacific site is located on the edge of the cold tongue in an area of large horizontal temperature gradients, while the location of the Western Pacific warm pool is slightly offset in HadCM3, meaning that in HadCM3 the Western Pacific site is not representative of the Western Pacific warm pool. Because of these issues we do not perform a site to model gridbox model data comparison here. Instead we will consider the range of values that lie within 2.5° and 5° of the gridbox containing each site, which will ensure that both the cold tongue and the warm pool in HadCM3 are included.

Figure 6 shows the range of modelled values of $\delta^{18}O_c$ and temperature within 2.5° and 5° of the western Pacific warm pool region (shaded region) and the Eastern Pacific region (grey lines) for the pre-industrial simulation and the Pliocene simulation. $\delta^{18}O_c$ was obtained from modelled temperature and modelled $\delta^{18}O_{sw}$ using the equation of *Erez and Luz* (1983). Preindustrial $\delta^{18}O_c$ is in reasonable agreement with the core top values, which represent recent times, (-2.22‰ at site 806 and -1.42‰ at a location near site ODP847 *Dekens et al.*, 2002). However the modelled $\delta^{18}O_c$ at 3.2Ma is less than *Wara et al.* (2005) reported for site ODP806 (~ -1.5‰) or site 847 (~ -1.3‰). Despite this notable offset the measured gradients across the Pacific of 0.25‰ is within the large range of values that occur within 2.5° of the modelled sites, and the range of modelled temperatures is sufficiently large to capture the observations. In the model the temperature and $\delta^{18}O_c$ gradients at these locations, are similar for the two time periods. In agreement with *Wara et al.* (2005) the thermocline in the Eastern Pacific has changed little between the pre-industrial and the Pliocene; however we do not find changes in the E-W gradient of either temperature or $\delta^{18}O_c$. The main differences between the two time periods is a $\sim$ 0.5‰ decrease in $\delta^{18}O_c$ and a $\sim$ 2.0°C warming in the Pliocene which applies consistently to the top 100m of the ocean and at both sites. The model is unable to assess why some analyses show the Western Pacific was warmer in the Pliocene, while others do not. We are not able to collaborate suggestions by *Zhang et al.* (2014a), that some records could have been compromised by changes in seawater chemistry, diagenesis and callibration limitations. However we do note the $\delta^{18}O_c$ Pliocene data is up to 1.2‰ higher than in the model, while the model agrees well with data for recent times, opening the possibility that diagenesis may be affecting at least the $\delta^{18}O_c$ measurements.

The large temperature gradients across both sites and the strong Eastern Pacific thermocline means that a small shift in either the Warm Pool or the cold tongue could lead to a reduction in the gradient across the Pacific without a permanent El Niño. Although we do not see either feature shift in our simulations it is possible that a different (and equally valid) orbital configuration which occurred in the Pliocene may lead to such a shift. Attributing a reduced E-W gradient (based on a single Western Pacific site) to 'permanent' El Niño, may not

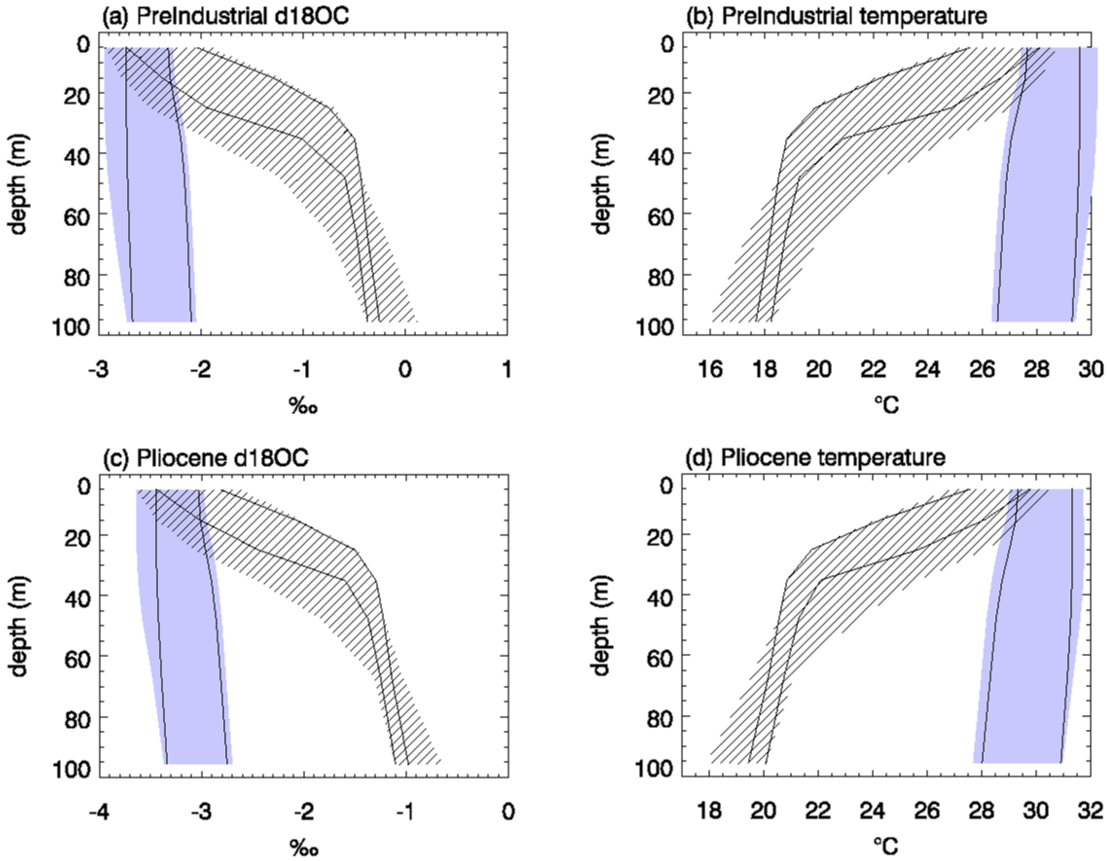

Figure 6: Modelled $\delta^{18}O_c$ and temperature representing the site ODP806 in the Western Pacific (shaded region), and ODP847 in the eastern Pacific (hatched region). The full range of values shown is model output within 5°C of the gridbox containing each site. The thin black lines highlight the range of values within 2.5° of the gridbox containing the site.

therefore be fully robust, even if the existence of such an E-W gradient was universally accepted.

5.2 Individual Foraminifera Analysis

The major limitation of using bulk foraminifera measurements to investigate El Niño for past climates is that interannual variability can not be measured. For example although bulk foraminifera measurements can suggest whether or not the average East-West temperature gradient in the Pliocene was different, they cannot indicate why these average differences occur. For example a smaller east-west average temperature gradient could be due to a) permanent "El Niño like" conditions b) ENSO variability around a smaller than modern East-West temperature gradient, or c) more frequent and stronger El Niño episodes imposed on a background state similar to modern. To overcome these issues an alternative way of analysing foraminifera was proposed by *Koutavas et al.* (2006). This analyses $\delta^{18}O_c$ measurements on a number of individual foraminifera, with a single foraminifera representing the climatic conditions for a

2-4 week period, and can show monthly variability. Any foraminifera representing temperatures that are warmer than would be expected in the warmest month or colder than would be expected in the coldest month could be classed as 'extra seasonal' and be attributed to ENSO related variability. This method has the disadvantage, in that it can only detect El Niño episodes that occur in the season where the temperature is warmest. For example, a very large El Niño in September would not show extraseasonal temperature in the Eastern Pacific region, since it would still be cooler than the average April temperature. The advantage to this method, however, is that some El Niño and La Niña events should be detected, provided enough individual foraminifera are used, and the presence of these events should be sufficient to state whether there was ENSO variability. Here we will use the HadCM3 simulations to investigate whether ENSO variability in the Pliocene can be detected in this way and compare results to the *Scroxton et al.* (2011) study which analysed individual foraminifera of Pliocene age to determine ENSO variability.

HadCM3 is used to simulate values of individual foraminifera $\delta^{18}O_c$ at the gridbox containing the ODP site 846 (3°S,90°W) that was used by *Scroxton et al.* (2011). This is shown for the Pliocene and the preindustrial in figure 7. Here each foraminifera $\delta^{18}O_c$ is calculated using the temperature and $\delta^{18}O_{sw}$ that occurred in a single month of the last 50 years of the simulation. Black crosses represent times when the model was in a neutral state, red crosses represent times when the model was in an El Niño state and blue crosses represent times when the model was in a La Niña state. Different depths have been shown to suggest what the results would be for different foraminifera species, and foraminifera representing El Niño and La Niña have been slightly offset for clarity. For the preindustrial (figure 7a), it can be seen that the extreme low $\delta^{18}O_c$ values represent times when the model is in an El Niño state, while the extreme high $\delta^{18}O_c$ values represent times when the model is in a La Niña state. This analysis suggests that, for the pre-industrial, extraseasonal events detected in Planktonic foraminifera species that live down to 130m, will represent El Niño and La Niña conditions.

For the Pliocene (figure 7b) the results are slightly different. In this case the times with extraseasonal high values of $\delta^{18}O_c$ still generally represent La Niña conditions, however the times of extraseasonal low values of $\delta^{18}O_c$ is less clear than the pre-industrial case. Indeed this figure suggests that in the top 30m of the ocean the times of greatest extraseasonal low values of $\delta^{18}O_c$ are associated with La Niña which is contrary to expectations. Although both extraseasonal high and low values of $\delta^{18}O_c$ are reproduced by the Pliocene simulation, without prior knowledge it would be impossible to accurately determine El Niño events from the simulated foraminifera data. In order to check that the last 50 years of the Pliocene simulation were typical, we repeated this analysis for the preceding 50 years of the Pliocene simulation and found similar results. However in the preceding 50 years (not shown) extraseasonal low values of modelled $\delta^{18}O_c$, at the time of La Niña, were also obtained down to the 130m depth.

To understand why the model suggests it possible to detect extraseasonal El Niño events in the pre-industrial, but not in the Pliocene, at this site we will first consider the component parts of the modelled foraminifera $\delta^{18}O_c$, namely $\delta^{18}O_{sw}$ and temperature. We will consider the surface and also the next layer (10-20m) where the extraseasonal low values occurring at the time of a La Niña are highest.

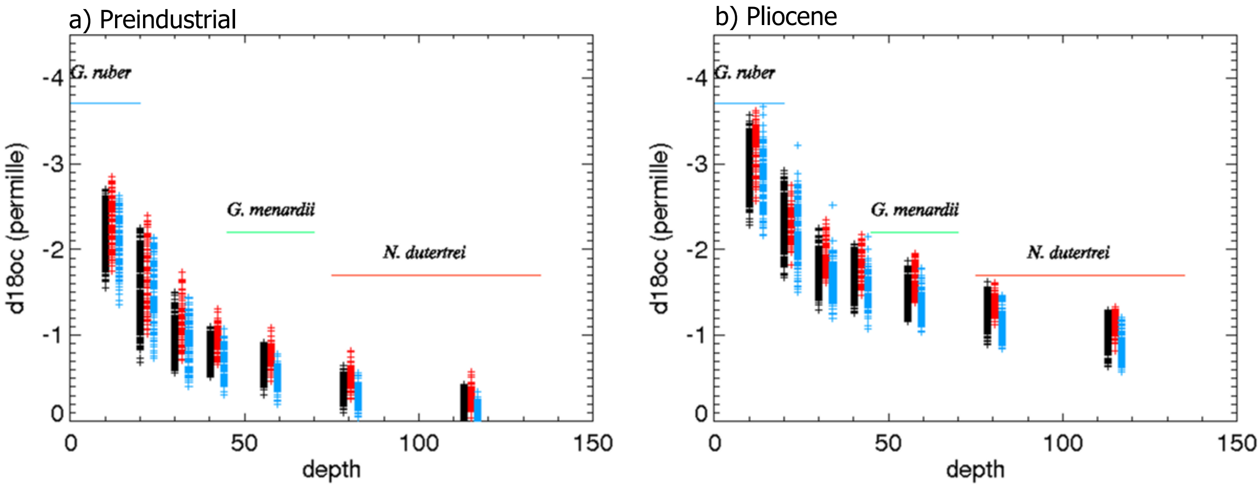

Figure 7: Modelled individual foraminifera from the last 50 years of the pre-industrial (left) and Pliocene (right) simulations. Black crosses represent times when the model was in a neutral state, red crosses represent times when the model was in an 'El Niño' state and blue crosses represent times when the model was in a La Niña state. Different depths have been shown to suggest what the results would be for different foraminifera species.

Figure 8a shows a timeseries of monthly averaged temperature, $\delta^{18}O_{sw}$ and $\delta^{18}O_c$ for the last 50 years of the pre-industrial simulation. Times where the model is in an El Niño state are shown in red, times when the model is in a La Niña state are shown in blue and neutral conditions are shown in black. Horizontal lines have been overplotted at arbitrary limits of 28°C for temperature, 0.7‰ for $\delta^{18}O_{sw}$ and -2.6‰ for $\delta^{18}O_c$ to highlight where the extreme values occur. In agreement with figure 7 we see that the times of lowest $\delta^{18}O_c$ values occur during El Niño conditions, the highest $\delta^{18}O_c$ occur during La Niña condition and extraseasonal values are correctly attibuted. The low values of $\delta^{18}O_c$ that are detected as El Niño are all due to warm temperatures and $\delta^{18}O_{sw}$ varies little. Figure 8b shows the analogous timeseries for the Pliocene simulation. Although generally the highest temperature values occur at the time of an El Niño and the lowest temperature values occur at the time of a La Niña these results do not always follow through into $\delta^{18}O_c$. Indeed the most extreme low values of $\delta^{18}O_c$ occur around months 16-17 at a time of La Niña (see also extreme value at 10m on figure 7b). In addition some true El Niño episodes which cause extreme values in temperature do not translate to extreme values in $\delta^{18}O_c$ (see near month 200). These errors are partly due to temperature (which will be discussed later) and partly due to changes in $\delta^{18}O_{sw}$. Comparing figures 8a and 8b we see that $\delta^{18}O_{sw}$ at this site was much more variable in the Pliocene. Variability in $\delta^{18}O_{sw}$ is not obviously tied to the phase of ENSO, however an extreme low value of $\delta^{18}O_{sw}$ (such as occurs at months 16-17) can amplify a small peak in temperatures at this time to produce a very low value of $\delta^{18}O_c$. This low value would be falsely interpreted (from figure 7b alone) as the strongest El Niño in the record. Large $\delta^{18}O_{sw}$ variability that is not obviously tied to ENSO can therefore interfere with the signal in archived $\delta^{18}O$, which is being used to understand ENSO. The reason that $\delta^{18}O_{sw}$ in this region is more variable in the Pliocene than in the pre-industrial is mainly because the hydrological cycle is stronger in the Pliocene. Peak values of precipitation in this region are typically 40% larger in the Pliocene and act to supply reduced $\delta^{18}O_p$ to the ocean, which in turn reduces $\delta^{18}O_{sw}$. In a month of large precipitation the

δ^{18}O of the precipitation entering the ocean can be $\sim -10‰$ and can lower the $\delta^{18}O_{sw}$ from its typical value of $\sim 0.5‰$. The lowest value of $\delta^{18}O_{sw}$ ($\sim -0.8‰$) seen at months 16-17 in figure 8 corresponds to the largest precipitation value in this timeseries which has the lowest $\delta^{18}O_p$ value.

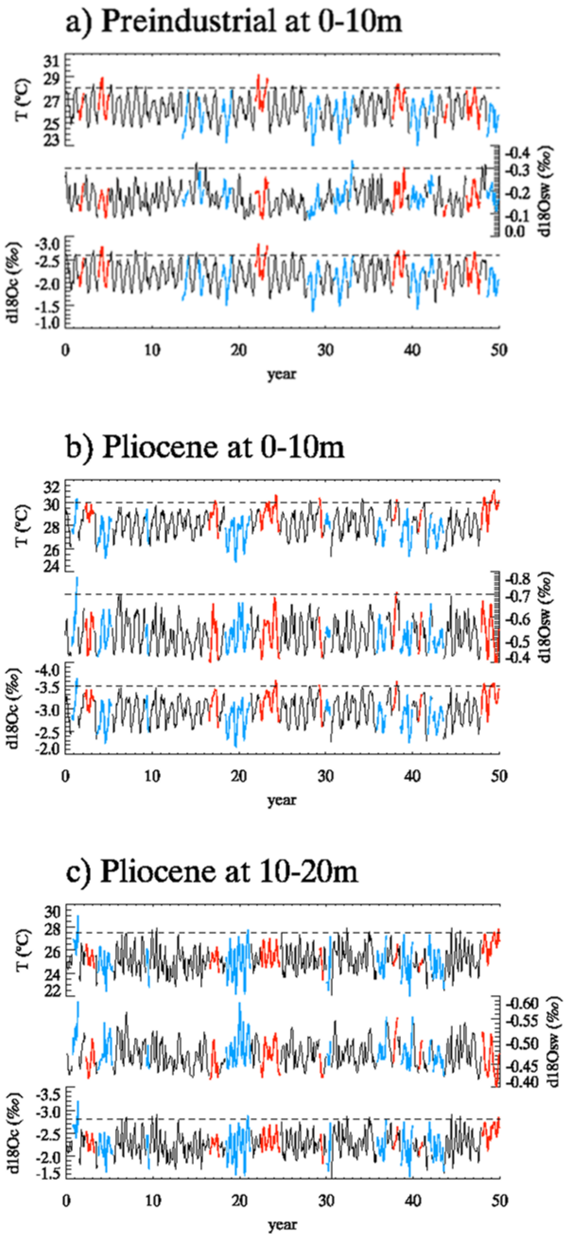

Figure 8: Temperature, $\delta^{18}O_{sw}$ and $\delta^{18}O_c$ from the last 50 years of the simulations. Red (blue) shows times when the model is in an El Niño (La Niña) state. Horizontal lines are drawn on each figure to highlight 'extreme' events.

Although $\delta^{18}O_{sw}$ is clearly important for the surface ocean $\delta^{18}O_c$, at deeper levels its importance is diminished. This is because $\delta^{18}O_{sw}$ is less variable at deeper levels because precipitation and evaporation will have largest effect near the ocean surface. Indeed at the 10-20m model level the variability in $\delta^{18}O_{sw}$ is typically half what it is at the 0-10m model level. We noted previously that at the surface both $\delta^{18}O_{sw}$ and temperature were responsible for producing the unexpected low values of $\delta^{18}O_c$. The La Niña in months 16-17 appeared extraseasonal at the surface mainly because of the anomolous $\delta^{18}O_{sw}$, but this La Niña was also uncharacteristically warm in this gridbox. At deeper ocean levels, where the unexpected low $\delta^{18}O_c$ values in a La Niña month persist, $\delta^{18}O_{sw}$ varies less and temperature becomes relatively more important. Figure 8c shows temperature, $\delta^{18}O_{sw}$ and $\delta^{18}O_c$ for the final 50 years of the Pliocene experiment from the 10-20m layer of the ocean. At 10-20m, unlike the surface layer, El Niño neither has warm temperatures or low $\delta^{18}O_c$ at this location. At this location, the highest temperatures and highest $\delta^{18}O_c$ do not represent El Niño, but instead represent either La Niña or neutral conditions, and the IFA method could not correctly attribute the low extraseasonal values of $\delta^{18}O_c$ to El Niño. The warm values that occur near this site during some La Niña episodes are localised and do not reflect large scale conditions. They are due to a small region of ocean downwelling in the Eastern Pacific that occurs in April in the Pliocene simulation. Small interannual shifts in this region of downwelling occur and can infrequently lead to high localised temperatures in the subsurface Eastern Pacific waters. It is unclear whether this small region of downwelling in the Pliocene simulation is reasonable or whether it is simply an artifact of the model. However, this example highlights that it is possible for non-ENSO related features to affect a local site in the Pliocene, but not in the modern, and this could make a method which appears suitable for ENSO detection based on modern data unsuitable for other time periods.

5.3 Which regions can ENSO be detected in IFA measurements?

In the same way that the model could simulate pseudo-corals from a large range of locations (see section 4.1), we can extend the planktonic foraminifera analysis to assess the IFA technique throughout the Pacific. We use the final 300 years of data from the simulation and simulate monthly individual foraminifera measurements for the surface, for each gridbox across the Pacific.

Scroxton et al. (2011) calculated that the probablity of a month occurring with conditions that would be recorded as extraseasonal for *G. ruber*, the surface dwelling species, was 0.04. Following this we classify the lowest and highest 2% of simulated foram $\delta^{18}O_c$ as extraseasonal. Gridboxes which have high precipitation or warm temperatures in El Niño years are expected to simulate the lowest 2% of $\delta^{18}O_c$ values when there is an El Niño and the highest 2% of values when there is La Niña (see figure 1). Gridboxes which are dry in El Niño years are expected to simulate the highest 2% of $\delta^{18}O_c$ values when there is an El Niño and the lowest 2% of values when there is La Niña. For each gridbox the fraction of extraseasonal events, which occur when the model is in the correct El Niño or La Niña state, is determined and results shown in figure 9. Only gridboxes where the extraseasonal events are correctly attributed in at least half of cases are plotted.

As with the timeseries data (represented by coral; figure 5), results from planktonic foraminifera data are similar for the Pliocene and the preindustrial. In general regions where a high fraction of extraseasonal values can be correctly attributed for the modern can also be correctly attributed for the Pliocene. However, as has been seen in the preceeding sections, this is not always the case, and care must be taken when considering individual gridboxes. In particular the Easternmost part of the Pacific (including near the *Scroxton et al.* (2011) site, which is marked) shows a much reduced skill in the Pliocene relative to the preindustrial. As shown above this is due to more non-ENSO related variability (such as in $\delta^{18}O_{sw}$), and shifts in upwelling zones. It is probable that these shifts in upwelling zones are an artefact of the model and do not represent true Pliocene conditions. If this is the case the reduced skill in this region for the Pliocene will not represent reality. However, this does highlight the fact that a single location can be subject to significant variability that is not related to ENSO, and without a continuous timeseries to analyse, short term variability can strongly effect a signal. Note that for the modelled continuous timeseries (represented by pseudocorals; figure 5) the Eastern Pacific has greater skill in the Pliocene than in the preindustrial. With continuous timeseries data, a single anomalous month is not able to incorrectly infer an ENSO event.

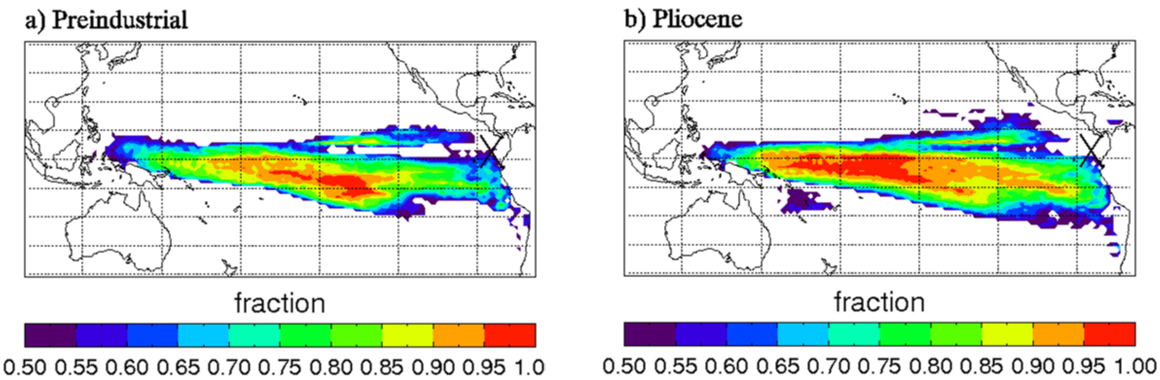

Figure 9: Fraction of the most extreme 2% of pseudo planktonic foraminifera measurements that were correctly attributed to El Niño and La Niña for each location across the Pacific.

Figure 9 shows the modelled results from the gridbox containing the *Scroxton et al.* (2011) site are not typical throughout the Pacific. Overall the fraction of extraseasonal values that are El Niño or La Niña is greater in the Pliocene than it is for the Preindustrial. In agreement with the pseudocoral data, the central Pacific is a particularly good region for ENSO detection, both for the Pliocene and the preindustrial. The Western Pacific, (near Papua New Guinea) is the region that shows the greatest increase in skill in the Pliocene. This is due to the fact that this region has an ENSO related precipitation signal, which is much stronger in the Pliocene than in the preindustrial (see figure 1), while the ENSO related temperature change between the two climates is relatively smaller.

6 Conclusions

In the simulations discussed here, the amplitude of El Niño was larger in the Pliocene than the preindustrial, and the hydrological cycle (both ENSO related and non-ENSO related) was stronger. This difference in ENSO behaviour can affect the accuracy of ENSO detection from paleoarchives. If ENSO was instead weaker in the Pliocene as suggested by other models (*Brierley*, 2015, *Zhang et al.*, 2013), or for certain times and locations (*Tindall et al.*, 2016) results are likely to differ. In our study the increased magnitude of El Niño can be seen in all the fields we considered (temperature, precipitation, $\delta^{18}O_p$ and $\delta^{18}O_{sw}$), and this makes El Niño easier to detect in Pliocene proxy data than it would be in proxy data from recent times. Two types of pseudo data produced from the HadCM3 model were considered to assess whether ENSO could be detected and for which regions this detection was accurate,

The first type of data considered was HadCM3 derived 'pseudo-corals' which were intended to represent archives where a continuous time series with high temporal resolution could be available, such as coral or Mollusk data. For completeness a pseudo-coral was produced for each gridbox in the tropical Pacific, even though the potential for such data to exist is limited to a small number of localities. Looking at individual localities where a strong ENSO signal was expected, it was found that the skill of accurately detecting ENSO was slightly larger in the Pliocene than in the Preindustrial (due to the stronger El Niño signal in the Pliocene). However this slight increase in skill between the two time periods was relatively modest when compared with the large variation in skill due to location. In general, areas which have a good skill at ENSO detection in the preindustrial also have good skill in the Pliocene, however the region is slightly expanded in the Pliocene. The reasoning of *Watanabe et al.* (2011), which compared Pliocene coral with a nearby live coral, to assess ENSO behaviour is supported by our study.

Modelling $\delta^{18}O_{sw}$ cannot always help reconcile model and data. This was shown by using the HadCM3 model to assess the change in the east-west gradient across the Pacific that was discussed by *Wara et al.* (2005) study. Although the data shows a decrease in the temperature and $\delta^{18}O_c$ gradients across the tropical Pacific between the Pliocene and the pre-industrial this could not be reproduced with the model. This could be due to factors such as model boundary conditions only representative of a short Pliocene timeslice while the bulk foraminifera measurements represent a much longer time period. However our analysis highlighted that both temperature and $\delta^{18}O_c$ were subject to large spatial gradients in these regions and suggested that a shift in climate zones could explain the data without the requirement of a permanant El Niño.

The model results shown here provided interesting insights into using individual foraminifera to detect El Niño. It was found that for an individual location the results between the modern climate and the Pliocene climate could be decoupled such that El Niño could be detected in recent data, but not in the Pliocene data. However we acknowledge the limitations of considering model output from a single model gridbox, and do not claim that any location should necessarily be avoided for ENSO studies. Instead we highlight that there could be different processes occurring in the Pliocene and that validating the IFA method using modern data may not mean that this method is suitable for other periods. This is in contrast to what we suggested for timeseries data (such as coral), as in timeseries data a non-ENSO anomaly would have to persist for several months to affect the results.

Despite the Pliocene simulation suggesting that the IFA technique could be unreliable for the Pliocene near the Eastern Pacific datasite available (*Scroxton et al.*, 2011), results based on this method were generally encouraging. Across most of the Pacific this technique had greater skill in accurately attributing extraseasonal events to El Nino and La Nina conditions for the Pliocene than for the preindustrial. In the central and western central Pacific the skill was particularly improved.

Throughout this paper the central Pacific has been highlighted as one region where paleoproxies are likely to provide a good signal of ENSO variability. Data which has a continuous time series (like corals) and data which has high resolution but is not continuous (like individual foraminifera) both perform well in this region. The model suggests that if data from this region provides an indication of ENSO activity, there is good confidence that El Niño, La Niña and neutral conditions are correctly attributed. This is not the case in all regions, and we have highlighted cases where strong ENSO activity has been falsely implied. If we can be confident that the data is accurately categorising ENSO, it would then be useful to use the data determine whether El Niño was stronger, weaker or of similar magnitude in the Pliocene. This would then provide a suggestion of what ENSO may be like in a warm future climate.
THIS IS WHERE WE PUT THE CONCLUSIONS FROM KAU'S WORK.

In our simulations the Pliocene hydrological cycle was enhanced, and non ENSO related precipitation was also enhanced. The implications of this are twofold. Firstly, in a region that is influenced by ENSO, but with little other interannual variability, ENSO should be easier to detect than in the modern. Secondly, non-ENSO related interannual variability could be stronger in the Pliocene climate and this may mask the ENSO signal in Pliocene data even if it does not in the modern. This highlights the importance of considering all periods of variability when interpreting data from a single site.

ACKNOWLEDGEMENTS: THank Watanabe.

References

AchutaRao, K., and K. R. Sperber (2002), Simulation of the El Nino Southern Oscillation: Results from the Coupled Model Intercomparison Project, *Clim. Dyn.*, *19*(3-4), 191–209.

Bellenger, H., E. Guilyardi, J. Leloup, M. Lengaigne, and J. Vialard (2014), ENSO representation in climate models: from CMIP3 to CMIP5, *Clim. Dyn.*, *42*(7-8), 1999–2018, doi:10.1007/s00382-013-1783-z.

Bonham, S. G., A. M. Haywood, D. J. Lunt, M. Collins, and U. Salzmann (2009), El Nino-Southern Oscillation, Pliocene climate and equifinality, *PHILOSOPHICAL TRANSACTIONS OF THE ROYAL SOCIETY A-MATHEMATICAL PHYSICAL AND ENGINEERING ScienceS*, *367*(1886), 127–156, doi:10.1098/rsta.2008.0212.

Bragg, F. J., D. J. Lunt, and A. M. Haywood (2012), Mid-Pliocene climate modelled using the UK Hadley Centre Model: PlioMIP Experiments 1 and 2, *Geosci. Model Dev.*, *5*(5), 1109–1125, doi:10.5194/gmd-5-1109-2012.

Brierley, C. M. (2015), Interannual climate variability seen in the Pliocene Model Intercomparison Project, *Climate of the Past*, *11*(3), 605–618.

Collins, M., S.-I. An, W. Cai, A. Ganachaud, E. Guilyardi, F.-F. Jin, M. Jochum, M. Lengaigne, S. Power, A. Timmermann, G. Vecchi, and A. Wittenberg (2010), The impact of global warming on the tropical Pacific ocean and El Nino, *Nature Geoscience*, *3*(6), 391–397, doi:10.1038/NGEO868.

Cox, P., R. A. Betts, C. B. Bunton, R. L. H. Essery, P. R. Rowntree, and J. Smith (1999), The impact of new land surface physics on the GCM simulation of climate and climate sensitivity, *Clim. Dyn.*, *15*(3), 183–203.

Dai, A., and T. M. L. Wigley (2000), Global patterns of ENSO-induced precipitation, *Geophys. Res. Lett.*, *27*(9), 1283–1286.

Dee, S., D. Noone, N. Buenning, J. Emile-Geay, and Y. Zhou (2015), SPEEDY-IER: A fast atmospheric GCM with water isotope physics, *JOURNAL OF GEOPHYSICAL RESEARCH-ATMOSPHERES*, *120*(1), 73–91, doi:10.1002/2014JD022194.

Dekens, P., D. Lea, D. Pak, and H. Spero (2002), Core top calibration of Mg/Ca in tropical foraminifera: Refining paleotemperature estimation, *GEOCHEMISTRY GEOPHYSICS GEOSYSTEMS*, *3*, doi:10.1029/2001GC000200.

Dolan, A. M., A. M. Haywood, D. J. Hill, H. J. Dowsett, S. J. Hunter, D. J. Lunt, and S. J. Pickering (2011), Sensitivity of Pliocene ice sheets to orbital forcing, *Palaeogeogr. Palaeoclimatol. Palaeoecol.*, *309*(1-2), 98–110.

Dowsett, H., R. Thompson, J. Barron, T. Cronin, F. Fleming, S. Ishman, R. Poore, D. Willard, and T. Holtz (1994), Joint Investigations of the Middle Pliocene Climate. 1. PRISM paleoenvironmental reconstructions, *Glob. Planet. Chang.*, *9*(3-4), 169–195.

Dowsett, H., M. Robinson, A. Haywood, U. Salzmann, D. Hill, L. Sohl, M. Chandler, M. Williams, K. Foley, and D. Stoll (2010), The PRISM3D paleoenvironmental reconstruction, *Stratigraphy*, *7*(2-3), 123–139.

Edwards, J. M., and A. Slingo (1996), Studies with a flexible new radiation code. 1. Choosing a configuration for a large-scale model, *Q. J. R. Meteorol. Soc.*, *122*(531), 689–719.

Erez, J., and B. Luz (1983), Experimental paleotemperature equation for planktonic-foraminifera, *Geochim. Cosmochim. Acta.*, *47*(6), 1025–1031.

Fedorov, A., P. Dekens, M. McCarthy, A. Ravelo, P. deMenocal, M. Barreiro, R. Pacanowski, and S. Philander (2006), The Pliocene paradox (mechanisms for a permanent El Nino), *Science*, *312*(5779), 1485–1489, doi:10.1126/science.1122666.

Goddard, L., and M. Dilley (2005), El Nino: Catastrophe or opportunity, *JOURNAL OF CLIMATE*, *18*(5), 651–665, doi:10.1175/JCLI-3277.1.

Gordon, C., C. Cooper, C. Senior, H. Banks, J. Gregory, T. Johns, J. Mitchell, and R. Wood (2000), The simulation of SST, sea ice extents and ocean heat transports in a version of the Hadley Centre coupled model without flux adjustments, *Clim. Dyn.*, *16*(2-3), 147–168.

Gregory, D., and D. Morris (1996), The sensitivity of climate simulations to the specification of mixed phase clouds, *Clim. Dyn.*, *12*(9), 641–651.

Gregory, D., and P. R. Rowntree (1990), A mass flux convection scheme with representation of cloud ensemble characteristics and stability-dependent closure, *Mon. Weather Rev.*, *118*(7), 1483–1506.

Haese, B., M. Werner, and G. Lohmann (2013), Stable water isotopes in the coupled atmosphere-land surface model ECHAM5-JSBACH, *GEOSCIENTIFIC MODEL DEVELOPMENT*, *6*(5), 1463–1480, doi:10.5194/gmd-6-1463-2013.

Haywood, A. M., P. J. Valdes, and B. W. Sellwood (2000), Global scale palaeoclimate reconstruction of the middle Pliocene climate using the UKMO GCM: initial results, *Glob. Planet. Chang.*, *25*(3-4), 239–256.

Haywood, A. M., D. J. Hill, A. M. Dolan, B. L. Otto-Bliesner, F. Bragg, W. L. Chan, M. A. Chandler, C. Contoux, H. J. Dowsett, A. Jost, Y. Kamae, G. Lohmann, D. J. Lunt, A. Abe-Ouchi, S. J. Pickering, G. Ramstein, N. A. Rosenbloom, U. Salzmann, L. Sohl, C. Stepanek, H. Ueda, Q. Yan, and Z. Zhang (2013), Large-scale features of Pliocene climate: results from the Pliocene Model Intercomparison Project, *Clim. Past*, *9*(1), 191–209.

Haywood, A. M., P. J. Valdes, and V. L. Peck (2007), A permanent El Nino-like state during the Pliocene?, *Paleoceanography*, *22*(1), doi:10.1029/2006PA001323.

Haywood, A. M., A. M. Dolan, S. J. Pickering, H. J. Dowsett, E. L. McClymont, C. L. Prescott, U. Salzmann, D. J. Hill, S. J. Hunter, D. J. Lunt, J. O. Pope, and P. J. Valdes (2013), On the identification of a Pliocene time slice for data-model comparison, *Philos. T. Roy. Soc. A*, *371*(2001), doi:10.1098/rsta.2012.0515.

Hill, D. J. (2015), The non-analogue nature of Pliocene temperature gradients, *EARTH AND PLANETARY SCIENCE LETTERS*, *425*, 232–241, doi:10.1016/j.epsl.2015.05.044.

Holmes, J. A., J. Tindall, N. Roberts, W. Marshall, J. D. Marshall, A. Bingham, I. Feeser, M. O'Connell, T. Atkinson, A.-L. Jourdan, A. March, and E. H. Fisher (2016), Lake isotope records of the 8200-year cooling event in western Ireland: Comparison with model simulations, *QUATERNARY SCIENCE REVIEWS*, *131*(B), 341–349, doi:10.1016/j.quascirev.2015.06.027.

Juillet-Leclerc, A., and G. Schmidt (2001), A calibration of the oxygen isotope paleothermometer of coral aragonite from Porites, *Geophys. Res. Lett.*, *28*(21), 4135–4138.

Koutavas, A., P. B. deMenocal, G. C. Olive, and J. Lynch-Stieglitz (2006), Mid-Holocene El Nino-Southern Oscillation (ENSO) attenuation revealed by individual foraminifera in eastern tropical Pacific sediments, *GEOLOGY*, *34*(12), 993–996, doi:10.1130/G22810A.1.

Latif, M., and N. S. Keenlyside (2009), El Nino/Southern Oscillation response to global warming, *PROCEEDINGS OF THE NATIONAL ACADEMY OF SCIENCES OF THE UNITED STATES OF AMERICA*, *106*(49), 20,578–20,583, doi:10.1073/pnas.0710860105.

Lee, J.-E., I. Fung, D. J. DePaolo, and C. C. Henning (2007), Analysis of the global distribution of water isotopes using the NCAR atmospheric general circulation model, *J. Geophys. Res-Atmos.*, *112*(D16), doi:10.1029/2006JD007657.

Leloup, J., M. Lengaigne, and J.-P. Boulanger (2008), Twentieth century ENSO characteristics in the IPCC database, *Clim. Dyn.*, *30*(2-3), 277–291, doi:10.1007/s00382-007-0284-3.

Li, J., S.-P. Xie, E. R. Cook, G. Huang, R. D'Arrigo, F. Liu, J. Ma, and X.-T. Zheng (2011), Interdecadal modulation of El Nino amplitude during the past millennium, *Nature Climate Change*, *1*(2), 114–118, doi:10.1038/NCLIMATE1086.

Molnar, P., and M. Cane (2002), El Nino's tropical climate and teleconnections as a blueprint for pre-Ice Age climates, *Paleoceanography*, *17*(2), doi:10.1029/2001PA000663.

Philander, S., and A. Fedorov (2003), Role of tropics in changing the response to Milankovich forcing some three million years ago, *Paleoceanography*, *18*(2), doi:10.1029/2002PA000837.

Pope, V., M. Gallani, P. Rowntree, and R. Stratton (2000), The impact of new physical parametrizations in the Hadley Centre climate model: HadAM3, *Clim. Dyn.*, *16*(2-3), 123–146.

Pound, M. J., J. Tindall, S. J. Pickering, A. M. Haywood, H. J. Dowsett, and U. Salzmann (2014), Late Pliocene lakes and soils: a global data set for the analysis of climate feedbacks in a warmer world, *Clim. Past*, *10*(1), 167–180, doi:10.5194/cp-10-167-2014.

Prescott, C. L., A. M. Haywood, A. M. Dolan, S. J. Hunter, J. O. Pope, and S. J. Pickering (2014), Assessing orbitally-forced interglacial climate variability during the mid-Pliocene Warm Period, *Earth. Planet. Sci. Lett.*, *400*, 261–271.

Ravelo, A. C., K. T. Lawrence, A. Fedorov, and H. L. Ford (2014), Comment on "A 12-million-year temperature history of the tropical Pacific Ocean", *SCIENCE*, *346*(6216), doi:10.1126/science.1257618.

Roberts, C. D., A. N. LeGrande, and A. K. Tripati (2011), Sensitivity of seawater oxygen isotopes to climatic and tectonic boundary conditions in an early Paleogene simulation with GISS ModelE-R, *Paleoceanography*, *26*, doi:10.1029/2010PA002025.

Roche, D. M. (2013), delta O-18 water isotope in the iLOVECLIM model (version 1.0) - Part 1: Implementation and verification, *GEOSCIENTIFIC MODEL DEVELOPMENT*, *6*(5), 1481–1491, doi:10.5194/gmd-6-1481-2013.

Salzmann, U., A. M. Dolan, A. M. Haywood, W. L. Chan, J. Voss, D. J. Hill, A. Abe-Ouchi, B. Otto-Bliesner, F. J. Bragg, M. A. Chandler, C. Contoux, H. J. Dowsett, A. Jost, Y. Kamae, G. Lohmann, D. J. Lunt, S. J. Pickering, M. J. Pound, G. Ramstein, N. A. Rosenbloom, L. Sohl, C. Stepanek, H. Ueda, and Z. S. Zhang (2013), Challenges in quantifying Pliocene terrestrial warming revealed by data-model discord, *Nat. Clim. Chang.*, *3*(11), 969–974.

Scroxton, N., S. Bonham, R. E. M. Rickaby, S. H. F. Lawrence, M. Hermoso, and A. M. Haywood (2011), Persistent El Nino-Southern Oscillation variation during the Pliocene Epoch, *Paleoceanography, 26.*

Seki, O., G. L. Foster, D. N. Schmidt, A. Mackensen, K. Kawamura, and R. D. Pancost (2010), Alkenone and boron-based Pliocene pCO(2) records, *Earth and Planetary Science Letters*, *292*(1-2), 201–211, doi:10.1016/j.epsl.2010.01.037.

Seki, O., D. N. Schmidt, S. Schouten, E. C. Hopmans, J. S. S. Damste, and R. D. Pancost (2012), Paleoceanographic changes in the Eastern Equatorial Pacific over the last 10 Myr, *Paleoceanography*, *27*, doi:10.1029/2011PA002158.

Semtner, A. J. (1976), Model for thermodynamic growth of sea ice in numerical investigations of climate, *J. Phys. Oceanogr.*, *6*(3), 379–389.

Smith, R. N. B. (1990), A scheme for predicting layer clouds and their water-content in a general-circulation model, *Q. J. R. Meteorol. Soc.*, *116*(492), 435–460.

Stap, L. B., B. de Boer, M. Ziegler, R. Bintanja, L. J. Lourens, and R. S. W. van de Wal (2016), CO2 over the past 5 million years: Continuous simulation and new delta B-11-based proxy data, *EARTH AND PLANETARY SCIENCE LETTERS*, *439*, 1–10, doi:10.1016/j.epsl.2016.01.022.

Steph, S., R. Tiedemann, M. Prange, J. Groeneveld, M. Schulz, A. Timmermann, D. Nuernberg, C. Ruehlemann, C. Saukel, and G. H. Haug (2010), Early Pliocene increase in thermohaline overturning: A precondition for the development of the modern equatorial Pacific cold tongue, *PALEOCEANOGRAPHY*, *25*, doi:10.1029/2008PA001645.

Tindall, J., R. Flecker, P. Valdes, D. N. Schmidt, P. Markwick, and J. Harris (2010), Modelling the oxygen isotope distribution of ancient seawater using a coupled ocean-atmosphere GCM: Implications for reconstructing early Eocene climate, *Earth. Planet. Sci. Lett.*, *292*(3-4), 265–273, doi:10.1016/j.epsl.2009.12.049.

Tindall, J. C., and A. M. Haywood (2015), Modeling oxygen isotopes in the Pliocene: Large-scale features over the land and ocean, *PALEOCEANOGRAPHY*, *30*(9), 1183–1201, doi: 10.1002/2014PA002774.

Tindall, J. C., A. M. Haywood, and F. W. Howell (2016), Accounting for Centennial Scale variability when Detecting Changes in ENSO: A study of the Pliocene, *submitted to Paleoceanography.*

Tindall, J. C., P. J. Valdes, and L. C. Sime (2009), Stable water isotopes in HadCM3: Isotopic signature of El Nino Southern Oscillation and the tropical amount effect, *J. Geophys. Res-Atmos.*, *114*, doi:10.1029/2008JD010825.

von der Heydt, A. S., A. Nnafie, and H. A. Dijkstra (2011), Cold tongue/Warm pool and ENSO dynamics in the Pliocene, *Climate of the Past*, *7*(3), 903–915, doi:10.5194/cp-7-903-2011.

Wang, H., R. Zhang, J. Cole, and F. Chavez (1999), El Nino and the related phenomenon Southern Oscillation (ENSO): The largest signal in interannual climate variation, *PROCEEDINGS OF THE NATIONAL ACADEMY OF SCIENCES OF THE UNITED STATES OF AMERICA*, *96*(20), 11,071–11,072, doi:10.1073/pnas.96.20.11071.

Wara, M., A. Ravelo, and M. Delaney (2005), Permanent El Nino-like conditions during the Pliocene warm period, *Science*, *309*(5735), 758–761, doi:10.1126/science.1112596.

Watanabe, T., A. Suzuki, S. Minobe, T. Kawashima, K. Kameo, K. Minoshima, Y. M. Aguilar, R. Wani, H. Kawahata, K. Sowa, T. Nagai, and T. Kase (2011), Permanent El Nino during the Pliocene warm period not supported by coral evidence, *Nature*, *471*(7337), 209–211.

Winnick, M. J., J. M. Welker, and C. P. Chamberlain (2013), Stable isotopic evidence of El Nino-like atmospheric circulation in the Pliocene western United States, *Clim. Past*, *9*(5), 2085–2099.

Wittenberg, A. T. (2009), Are historical records sufficient to constrain ENSO simulations?, *Geophysical Research Letters*, *36*, doi:10.1029/2009GL038710.

Zhang, R., Q. Yan, R. S. Zhang, D. Jiang, B. L. Otto-Bliesner, A. M. Haywood, D. J. Hill, A. M. Dolan, C. Stepanek, G. Lohmann, C. Contoux, F. Bragg, W. L. Chan, M. A. Chandler, A. Jost, Y. Kamac, A. Abe-Ouchi, G. Ramstein, N. A. Rosenbloom, L. Sohl, and H. Ueda (2013), Mid-Pliocene East Asian monsoon climate simulated in the PlioMIP, *Clim. Past*, *9*(9), 903–912.

Zhang, Y. G., M. Pagani, and Z. Liu (2014a), A 12-Million-Year Temperature History of the Tropical Pacific Ocean, *Science*, *344*(6179), 84–87, doi:10.1126/science.1246172.

Zhang, Y. G., M. Pagani, and Z. Liu (2014b), Response to Comment on "A 12-million-year temperature history of the tropical Pacific Ocean", *SCIENCE*, *346*(6216), doi:10.1126/science.1257930.

Zhang, Z., Q. Yan, J. Z. Su, and Y. Q. Gao (2012), Has the Problem of a Permanent El Nio been Resolved for the Mid-Pliocene?, *Atmospheric and Oceanic Science Letters*, *5*(6), 445–448, doi:10.1080/16742834.2012.11447035.